ELSEVIER

Independent determination of the complex refractive index and wave impedance by time-domain terahertz spectroscopy

H. Němec [a], F. Kadlec [a], P. Kužel [a,*], L. Duvillaret [b], J.-L. Coutaz [b]

[a] *Institute of Physics, Academy of Sciences of the Czech Republic, Na Slovance 2, 182 21 Prague 8, Czech Republic*
[b] *Laboratoire d'Hyperfréquences et de Caractérisation, Université de Savoie, 73376 Le Bourget du Lac Cedex, France*

Abstract

We present a method for simultaneous determination of the refractive index and wave impedance – or equivalently of the dielectric permittivity and magnetic permeability – of bulk samples. Two independent complex spectroscopic quantities required for an unambiguous evaluation are experimentally obtained by temporal windowing of time domain waveforms measured in the transmission or reflection geometry. We discuss several approaches that can be used for the evaluation of the complex refractive index and wave impedance; three are quantitatively analyzed and compared. Successful evaluation of the dielectric and magnetic dispersion then crucially depends on the accuracy of the wave impedance measurements.
© 2005 Elsevier B.V. All rights reserved.

1. Introduction

Since time-domain terahertz (THz) spectroscopy (TDTS) was first proposed [1], this technique has become very widespread in many branches of physics, including characterization of dielectric properties [2], investigation of ultrafast dynamics in semiconductors and solutions [3] and imaging and sensing applications [4]. Despite that, there is a lack of studies focusing on the characterization of magnetic properties of materials in the THz range. Most of the works [5–12] postulate that the system exhibits only a dielectric or only a magnetic behavior, but not both at the same time, i.e., the refractive index and wave impedance of materials are not considered as independent quantities. However, a variation of the dielectric permittivity and magnetic permeability in the same spectral range is likely to occur in rare-earth orthoferrites [5,6] ($YFeO_3$, $TmFeO_3$, etc.), uniaxial antiferromagnetic fluorides [7,8] (e.g., FeF_2, CoF_2 and MnF_2) and molecular magnets [9]. The magnetic resonances in these materials are usually very narrow while the dielectric resonances are much broader. Using the above assumption the dielectric and magnetic character of resonances can be guessed.

At the same time, there is a rapidly growing interest in metamaterials and especially in so-called left-handed materials [13–17]. These structures are usually constructed as periodic arrays of metal wires and split-ring resonators. More recently a composite material consisting of thin alternating layers with dielectric and magnetic properties [18] has been proposed. Despite the discrete nature of these artificial materials on the sub-wavelength scale, they can be considered as continuous media on the scale of the probing wavelength. Consequently, they can be described by effective dielectric and magnetic susceptibilities which exhibit a dispersion within the same spectral range. Indeed, in this case the refractive index and the wave impedance are independent spectral functions, the left-handedness being attributed to the negative sign of the refractive index [13]. Thus, the simultaneous determination of these two complex quantities is essential to demonstrate the left-handedness of a metamaterial. The need for reliable methods capable of simultaneous determination of effective dielectric and magnetic functions in the THz range is further

---

* Corresponding author. Tel.: +420 266 052 176; fax: +420 286 890 527.
  E-mail address: kuzelp@fzu.cz (P. Kužel).

urged by the recent demonstrations by Yen et al. [19] and Moser et al. [20] of metamaterials exhibiting a negative effective magnetic permeability in this spectral range.

Up to now, only little attention has been paid to a complete dielectric and magnetic characterization of metamaterials: usually, only an enhanced power transmission is observed in the spectral range where the left-handed behavior is expected. However, as emphasized by Aydin et al. [21], the plasma edge of the array of wires may exhibit an appreciable red-shift in the presence of split-ring resonators. Consequently, the existence of an enhanced transparency region does not provide an unambiguous evidence of the left-handed behavior. A method of the determination of effective dielectric and magnetic functions from complex reflectance and transmittance spectra has been recently proposed in [22]. It can be useful for monochromatic spectroscopies, however, it was demonstrated using data obtained only from a numerical simulation.

In order to extend the application of the TDTS technique for investigating samples exhibiting both dielectric and magnetic properties, we develop in this paper methods useful for simultaneous determination of both refractive index and wave impedance from TDTS measurements assuming they are independent. Three representative approaches are validated by characterization of three non-magnetic samples and by characterization of a sample displaying a weak sharp magnon in the spectra, which allows to discuss the performance and applicability of these methods. Since all analytical expressions derived are not based on the assumption of nonmagnetic materials ($\mu = 1$), these methods can then be directly applied to materials displaying magnetic properties, with a proper knowledge of experimental errors.

The paper is structured as follows. In Section 2, we sum up basic concepts employed in this work – we describe the typical experimental setups and recall the principle of the determination of refractive index and wave impedance from the transmission and reflection measurements. In Section 3, we introduce and test experimentally the schemes aimed at simultaneous determination of dielectric and magnetic functions. These schemes are further discussed and their capabilities are compared with each other in Section 4. The contribution of this paper is finally summarized in Section 5.

2. Basic considerations

2.1. THz time-domain transmission and reflection spectroscopies

The principle of TDTS in the transmission configuration consists in measuring the temporal profile of the electric field of a picosecond THz pulse (THz waveform) transmitted by the sample. The complex frequency spectrum of this pulse is divided by that of the reference pulse (obtained when the sample is removed from the THz beam path) yielding the complex transmission function of the sample.

The multiple internal reflections of the THz beam in the sample appear as a series of mutually delayed echoes in the time-domain scan. The transmittance spectrum of the sample calculated from such a waveform (i.e., including all the internal reflections exceeding the noise level) is denoted as T. However, for sufficiently thick samples these echoes are separated in time. Thus TDTS allows one to take advantage of a temporal windowing procedure [23]: it is possible to determine experimentally the transmittance T_m corresponding to the echo leaving the sample after $2m$ internal reflections (e.g., T_0 is the transmission function corresponding to a direct pass without internal Fabry–Pérot reflections). These spectroscopic methods are well established and allow a precise determination of the dielectric function of the sample material [24–26].

The determination of the complex reflectance spectrum is analogous: the total complex reflectance R of the sample can be decomposed into a series of echoes separated in time and corresponding to the individual Fabry–Pérot contributions R_0, R_1, etc. The reference measurement is performed using a mirror with known characteristics. Appropriate care should be taken to determine the reflectance phase with good accuracy (see [27] and references therein).

Our experimental setup for the transmission measurements is a standard one similar to that employed in [28]. Our arrangement for the reflection measurements has been described in detail in [27]. In both experiments, the THz pulses are generated by a ZnTe [0 1 1] crystal via optical rectification of amplified femtosecond laser pulses (wavelength 800 nm, repetition rate 1 kHz) and focused onto the sample by ellipsoidal mirrors. The THz signal is detected in another ZnTe [0 1 1] crystal using the electro-optic effect and a standard polarization-sensitive optical detection system with balanced photodiodes [29].

2.2. Determination of refractive index and wave impedance

Determination of the complex permittivity ε and permeability μ – or equivalently complex refractive index $n = \sqrt{\varepsilon\mu}$ and relative wave impedance $z = \sqrt{\mu/\varepsilon}$ (called simply impedance in the following) – from spectroscopic measurements generally requires a knowledge of complex transmittance and reflectance spectra T and R. This is particularly true for monochromatic spectroscopic methods where the Fabry–Pérot reflections cannot be resolved in time. Such an approach has been described from the point of view of microwave applications in [22], and demonstrated on numerically calculated complex transmittance and reflectance spectra of metamaterials. In practice, this method is very sensitive to an accurate determination of the sample thickness as well as to a precise measurement of the spectra [30,10]. Recently, a similar approach has been also applied to the investigation of 1D photonic structures in the THz range yielding their characteristics with a good accuracy [31].

In contrast with frequency-domain methods, the TDTS has the advantage of phase sensitivity and the possibility of

temporal windowing. Therefore, in principle, it is sufficient to measure two independent complex spectral functions among the set of T_m's and R_m's in order to determine both n and z. Such an approach brings an important benefit: the dependence of T_m and R_m on n and z is much simpler compared to that of T and R and the extraction procedure is more direct and transparent. We show in the next section that the THz optical constants can be determined by an analytical calculation in many cases: this avoids problems with crossing of branches of mathematical solutions encountered when only R and T are considered [30].

This paper does not treat ellipsometry-like studies which, in principle, could also be convenient for determination of n and z. In such an experiment it would be necessary to measure R_0 for at least two angles of incidence and for two polarizations. Recently, experiments with a fixed incidence angle and a variable polarization were performed [32], and THz reflectance measurements with variable angle of incidence and a fixed polarization were also demonstrated [33]. To our knowledge the combination of both degrees of freedom has not been experimentally realized yet.

The lowest-order transmittance and reflectance functions for normal incidence read:

$$T_0(n,z) = \frac{4z}{(z+1)^2} \exp(2\pi i (n-1) f d/c), \qquad (1)$$

$$T_1(n,z) = T_0(n,z) \left(\frac{z-1}{z+1}\right)^2 \exp(4\pi i n f d/c), \qquad (2)$$

$$R_0(n,z) = \frac{z-1}{z+1}, \qquad (3)$$

where d is the thickness of the sample, f is the frequency, and c is the speed of light in vacuum. We always assume a planar wave formalism, linear electromagnetic response of the sample and its plane parallel shape. The polarization of the THz radiation is assumed to be linear and parallel to one of the principal axes of the sample (in the case of its optical anisotropy). We emphasize that expressions (1)–(3) have sense only if the temporal windowing of the picosecond THz pulses is possible. This means that the sample should be sufficiently thick, such that the echoes coming from internal reflections are separated in time. In practice, the condition $d \cdot \mathrm{Re}\, n \gtrsim 0.7$ mm is required for the temporal separation of the echoes. On the other hand, if a specific spectral resolution Δf is desired (e.g., in order to resolve some sharper features in the spectra) the inequality $d \cdot \mathrm{Re}\, n \gtrsim c/\Delta f$ must be fulfilled.

For non-magnetic samples (i.e., $\mu = 1$), z reduces to $1/n$. However, in the general case, z and n are independent and play very different roles in the transmission and reflection functions. The refractive index describes the electromagnetic propagation through the bulk of the sample. Its impact on the measured transmitted or reflected signal can be controlled by the choice of the sample thickness. In contrast, the impedance is introduced into the transmission and reflection formulas by a polynomial fraction term describing the impedance mismatch conditions at the interfaces.

At first, we focus on the dependence of the spectra corresponding to the direct pass (T_0 or R_0) on n and z. The generalization to higher order spectra is then straightforward.

Eqs. (1) and (3) are complex, i.e., they yield separate equations for the phase and equations for the amplitude of R_0 and T_0. The real part of the refractive index is mainly determined by the equation for the phase of T_0:

$$\mathrm{Re}\, n = 1 + \frac{c}{2\pi f d} \left(\arg T_0 + \arg \frac{(z+1)^2}{4z} + 2s\pi \right), \qquad (4)$$

where s is an integer. The values of the function arg are comprised between 0 and 2π. Note the existence of multiple branches of mathematical solutions of Eq. (4) which are spaced by 2π. The physically correct branch corresponding to a specific value of s has to be selected. This task has been addressed e.g., in [22,28,34] and is not of central importance in this paper. We only emphasize a simple fact that an increase of the sample thickness d is connected to an equivalent increase of the term $(\arg T_0 + 2s\pi)$ so that s is incremented each time when the value of $\arg T_0$ passes over the discontinuity at 2π. As the experimental error of $\arg T_0$ is independent of the sample thickness, the measurement of a very thick sample can provide a very accurate value of the real part of the refractive index [26]. This statement can be easily understood when samples with low losses ($\mathrm{Re}\, z \gg \mathrm{Im}\, z$) are considered: the term $\arg[(z+1)^2/4z]$ becomes negligible and the error in $\mathrm{Re}\, n$ obviously scales with $1/d$.

Analogously, the imaginary part of the refractive index is closely related to the equation for amplitude of T_0: its precision improves to some extent with increasing sample thickness, too. The best precision is obtained if the thickness of the sample approximately fulfills the condition $d \cdot \mathrm{Im}\, n \approx 0.05$ mm, which avoids excessive absorption losses in the spectral range 0.2–2.0 THz while keeping the maximum thickness possible.

The determination of the impedance can be most easily demonstrated for the case when the sample reflectance R_0 is available from the experiment. Eq. (3) is a simple algebraic equation for z independent of the sample thickness. Consequently, the precision of the extracted values of z is directly linked to the experimental error in R_0 (which depends merely on the performance of a particular experimental setup) and it cannot be improved by sample thickness optimization.

2.3. Selected experimental methods

Based on the choice of measured quantities T_m and/or R_m, several approaches for simultaneous determination of n and z can be devised. Our reflection setup [27] is very suitable for the determination of the reflectance R_0 corresponding to the main echo. On the other hand, due to a slightly oblique angle of incidence, higher order reflections

exhibit a lateral displacement of the beam leading to a decrease of accuracy. In this paper, we deal with the following representative methods:

Method A: Measurement of the transmittance and reflectance corresponding to the main echo (T_0 and R_0) is presented in Section 3.1.
Method B: Measurement of the transmittance corresponding to the main and to the first echo (T_0 and T_1) is treated in Section 3.2.
Method C: Measurement of the transmittances corresponding to the main echo for two samples with different thicknesses d_A and d_B ($T_{A,0}$ and $T_{B,0}$) is demonstrated in Section 3.3.

This list is not exhaustive. Approaches based on spectra corresponding to higher-order internal reflections can be naturally derived from this list, nevertheless we expect that potential advantages (lower noise, possibility of thickness refinement) [35] cannot bring at this stage significant improvement of the state of the art.

3. Experimental results

3.1. Transmittance and reflectance of the main echo

In the framework of this strategy, the set of equations is constructed from the reflectance and transmittance corresponding to the directly passing pulses. The equation for transmittance is particularly simple, as the measurement can be performed under normal incidence (see Eq. (1)). However, in the case of reflectance measurements, a slightly oblique incidence has to be usually used. The appropriate equation when using an *s*-polarized beam reads

$$R_0(n, z) = \frac{z \cos \theta_i - \sqrt{1 - \frac{\sin^2 \theta_i}{n^2}}}{z \cos \theta_i + \sqrt{1 - \frac{\sin^2 \theta_i}{n^2}}}, \tag{5}$$

where θ_i is the angle of incidence ($\theta_i \approx 12.5°$ in our setup). In order to determine the optical constants n and z, we solved the set of Eqs. (1) and (5) numerically. As it has been pointed out in Section 2.2, the numerical procedure provides several branches of mathematical solutions and the physically correct branch has to be selected.

However, note that Eq. (5) can be well approximated by Eq. (3) for small angles of incidence, allowing replacement of the numerical extraction procedure by an analytical one. In this case the impedance is determined from the measured reflectance spectrum using Eq. (3) and, subsequently, the refractive index is obtained using Eq. (1).

This approach was tested using a low-resistivity 0.885 mm thick (1 1 0)-oriented ZnTe crystal. The THz properties of the sample determined from the measured transmittance and reflectance spectra T_0 and R_0 are summarized in Fig. 1. Due to its small size the sample was fixed to an aperture with a diameter of 3.5 mm. The long-wavelength part
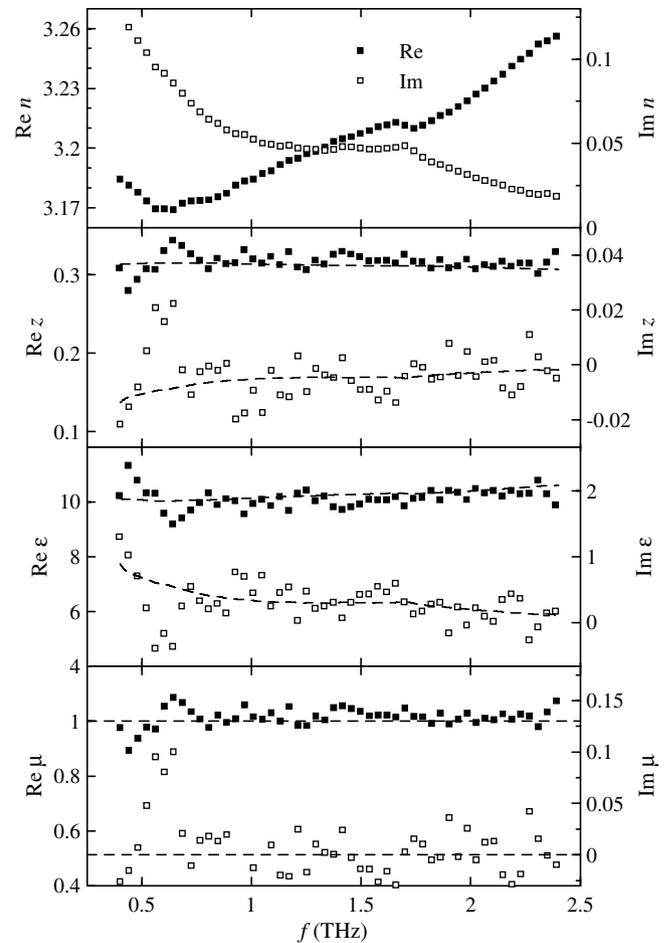

Fig. 1. Refractive index *n*, impedance *z*, permittivity ε and permeability μ of the investigated ZnTe sample, extracted from the transmittance and reflectance measurements corresponding to the main echo. Dashed lines correspond to the evaluation based on the measured complex refractive index (uppermost panel) and on the assumption of a non-magnetic sample (i.e., $\mu = 1$, $\varepsilon = n^2$, $z = 1/n$).

of the spectra then can be affected by diffraction effects and therefore it was removed from the data shown in Fig. 1. We can clearly observe the contribution of free carrier absorption in the plot of the complex refractive index. Moreover, around 1.7 THz, a weak superimposed resonance can also be identified. A similar feature near this frequency has been attributed to the TA(*X*) phonon [36]. Note, however, that both these features are relatively weak and that they are hidden by the noise in the plots of complex impedance. In agreement with the assumption of a non-magnetic response of ZnTe at THz frequencies, we find that the permeability fits well with the value $1 + 0i$.

Another material characterized by this method was the rare-earth orthoferrite TmFeO$_3$ [6]. The sample used was a 0.916 mm thick plane parallel plate. Its normal was parallel to the *b* crystallographic axis and it was oriented in the experiments so that the THz electric field was parallel to the *a*-axis. In this geometry, the THz spectra are expected to present a sharp antiferromagnetic mode at 0.7 THz [5]. As observed in Fig. 2 this very weak resonance is detected

in the spectrum of the complex refractive index. The variation of the refractive index induced by the antiferromagnetic mode corresponds approximately to 1% of the background value of Ren, thus exceeding the noise level by about an order of magnitude. In contrast, the resonance is too weak to be observed in the spectrum of the complex impedance.

As will be discussed later, the accuracy of the determination of the permittivity and permeability depends critically on the experimental error of the impedance spectrum. It is then clear that it is not possible to determine unambiguously whether the character of the observed mode is dielectric or magnetic from the measured data. It is worth evaluating how much the precision of the impedance determination has to be improved in order to enable the unambiguous determination of the observed mode. For this purpose we have performed a simultaneous fit of the measured n and z using a model of a magnetic spectrum presenting a single underdamped harmonic oscillator and a dielectric spectrum exhibiting a slow variation related to a tail of a higher-frequency phonon mode. The results of this fit along with the calculated permeability are shown in Fig. 2. Apparently the magnetic mode induces a variation in the impedance spectrum of about 1% of the value of Rez which is slightly below the noise level ($\approx$2%) observed in this part of the spectrum.

3.2. Transmittance of the main and the first echo

This approach consists of measuring the transmittances corresponding to the main pulse and to the first internal reflection, which are described by Eqs. (1) and (2), respec-

tively. The major advantages of this method are (i) the possibility of measurement under normal incidence, and (ii) the use of a single experimental setup instead of two considerably different ones as in Section 3.1. The determination of the sample THz properties is fully analytical: first, the impedance spectrum is determined from:

$$\frac{T_0^3 \exp(4\pi \mathrm{i} f d/c)}{T_1} = \left(\frac{4z}{z^2-1}\right)^2 \tag{6}$$

and, subsequently, the refractive index is obtained using Eq. (1).

Note that the measured waveform may contain parasitic echoes from the emitter, detector and other optics. These artifacts should be avoided unless the first sample echo is separated from them in time.

We validate this method using a (0001)-oriented 0.452 mm thick sapphire crystal. The results of our measurements are shown in Fig. 3. The refractive index exhibits a flat response in agreement with [24].

3.3. Transmittance of samples with different thicknesses

The last approach is based on a measurement of transmittances corresponding to the main echoes $T_{A,0}$ and $T_{B,0}$ of two samples with different thicknesses (d_A and d_B). The applicability of this method can sometimes be limited, since two samples of the same compound with different thicknesses should be available. The determination of the THz properties is based on a simultaneous inversion of two equations of the form (1) where d is replaced by d_A and d_B, respectively.
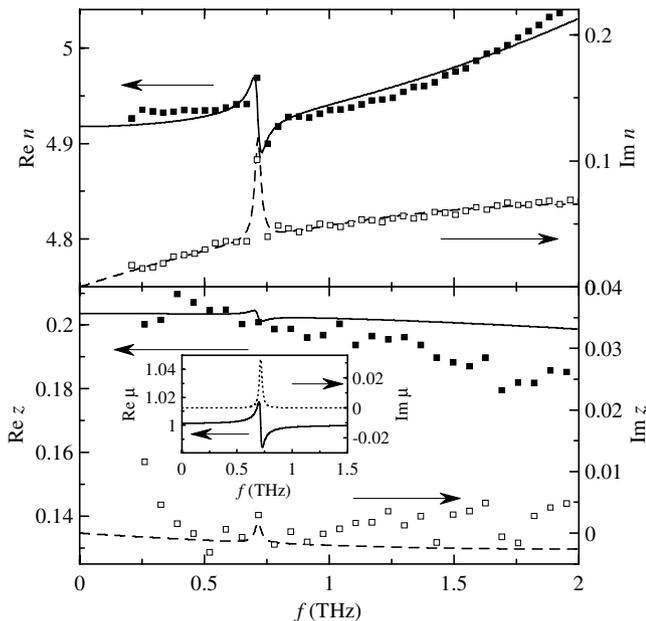

Fig. 2. Refractive index n and impedance z of TmFeO$_3$ extracted from the transmittance and reflectance measurements corresponding to the main echo; electric field $\|a$, magnetic field $\|c$. Lines: fit of the spectra assuming a sharp magnetic resonance and a slow dielectric variation corresponding to a tail of a phonon mode. Inset: resonance in the magnetic permeability resulting from the fit.
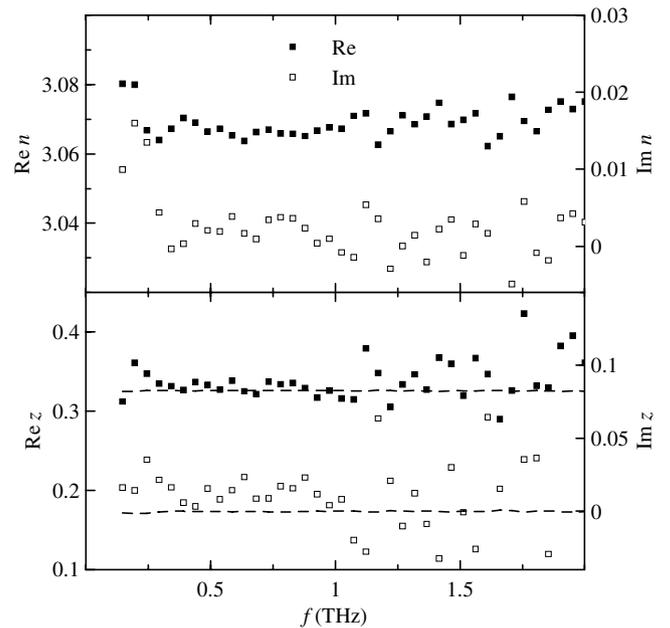

Fig. 3. Refractive index n and impedance z of the sapphire sample, extracted from the transmittance corresponding to the main echo and to the first internal reflection. Dotted lines correspond to the evaluation based on the measured complex refractive index (upper panel) and on the assumption of a non-magnetic sample ($\mu = 1$, i.e., $z = 1/n$).
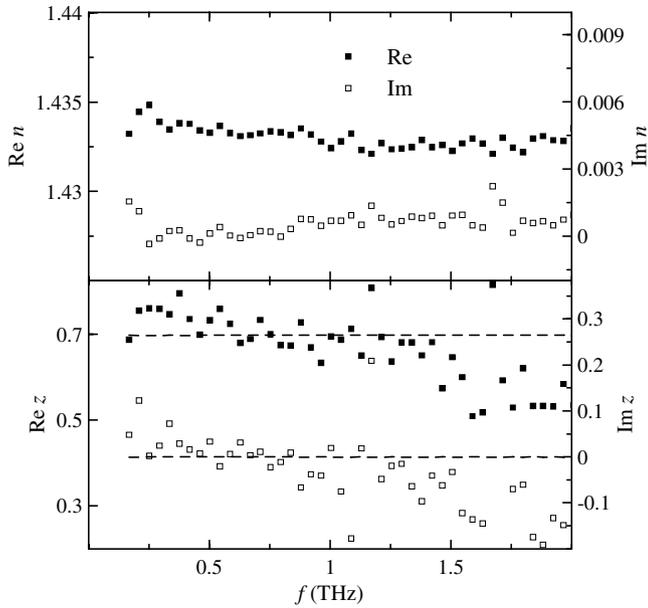
Fig. 4. Refractive index n and impedance z of the teflon sample, extracted from transmittance corresponding to main echoes of two samples with different thicknesses. The features around 1.2 and 1.7 THz are caused by water-vapor absorption. Dotted lines correspond to the evaluation based on the measured complex refractive index (upper panel) and on the assumption of a non-magnetic sample ($\mu = 1$, i.e., $z = 1/n$).

The calculations are straightforward as the ratio of transmittances $T_{A,0}/T_{B,0}$ directly yields a formula independent of the impedance:

$$\frac{T_{A,0}}{T_{B,0}} = \exp(2\pi i(n-1)f(d_A - d_B)/c), \tag{7}$$

while the impedance can be analytically obtained from:

$$(T_{B,0})^{\frac{d_A}{d_A - d_B}}(T_{A,0})^{\frac{d_B}{d_B - d_A}} = \frac{4z}{(z+1)^2}. \tag{8}$$

This method was checked using two teflon slabs with thicknesses 2.02 and 3.95 mm. The THz properties of the teflon determined by this method are displayed in Fig. 4. The flatness of the refractive index agrees very well with data published in [2].

4. Discussion

All the presented methods have several important characteristics in common. A brief inspection of plots of the refractive indices in Figs. 1–4 allows us to conclude that the refractive index can be determined very accurately, provided the determination of the sample thickness is accurate. The noise level of the data plotted in these Figures is smaller than 0.01, i.e., several tenths of a percent of the real part value. This can be understood keeping in mind the discussion exposed in Section 2.2. More quantitative insight into the problem can be obtained by differentiating Eqs. (1)–(3) with respect to the measured transmittances or reflectances, e.g., for the method A, one can write:

$$\Delta n = \left(\frac{\partial T_0}{\partial n}\right)^{-1}\Delta T_0 + \left(\frac{\partial R_0}{\partial n}\right)^{-1}\Delta R_0.$$

In this way one easily finds the following expressions for the relative errors of the complex refractive index:

$$\frac{\Delta n}{n} = \frac{c}{2\pi i f n d}\left(\frac{\Delta T_0}{T_0} + \frac{(1-z)^2}{2z}\frac{\Delta R_0}{R_0}\right) \tag{9}$$

for method A,

$$\frac{\Delta n}{n} = \frac{c}{2\pi i f n d}\left(\frac{6z - z^2 - 1}{2(1+z^2)}\frac{\Delta T_0}{T_0} + \frac{(1-z)^2}{2(1+z^2)}\frac{\Delta T_1}{T_1}\right) \tag{10}$$

for method B, and

$$\frac{\Delta n}{n} = \frac{c}{2\pi i f n(d_A - d_B)}\left(\frac{\Delta T_{A,0}}{T_{A,0}} - \frac{\Delta T_{B,0}}{T_{B,0}}\right) \tag{11}$$

for method C. ΔR_0 and ΔT_m are the errors of the measured reflectance and transmittance spectra, respectively. They involve both amplitude and phase error terms:

$$\frac{\Delta R_0}{R_0} = \frac{\Delta|R_0|}{|R_0|} + i\Delta\phi, \tag{12}$$

$$\frac{\Delta T_m}{T_m} = \frac{\Delta|T_m|}{|T_m|} + i\Delta\phi_m. \tag{13}$$

These terms are in general frequency dependent, increasing towards upper and lower ends of the spectra where R_0 and T_m vanish. A systematic phase error $\Delta\phi$, $\Delta\phi_j \propto f$ may also appear due to the time-domain jitter of the THz pulse position.

The important role of the sample thickness appears clearly in the expressions (9)–(11). The accuracy of the experimental value of the refractive index is significantly improved by a proper selection of the sample thickness. Note, however, that the precision of the refractive index as determined by method C is controlled by the thickness difference $d_A - d_B$ of the two samples used rather than by the sample thickness itself. Fig. 5(a) shows the variation of $\Delta n/n$ versus z (assuming that both n and z are real) at $f = 1$ THz and for the optical thicknesses nd and $n(d_A - d_B)$ equal to 0.7 mm. As observed, the experimental error is of the order of 0.1% for all the tested methods in agreement with the experimental results.

In contrast, the accuracy of the impedance spectra cannot be improved by a suitable selection of the sample thickness. The error in z is determined by the performance of the given setup, i.e., by the experimental error in the reflectance and transmittance spectra. These depend mainly on the scan-to-scan reproducibility of the signal and on the shot-to-shot noise of the femtosecond laser system; in the case of the reflectance measurements, it is also critically dependent on the correct reflectance phase determination. The sample thickness appears in Eqs. (6) and (8) as an additional parameter to be accurately determined; a possible error Δd in this parameter may further considerably decrease the accuracy of the impedance value.
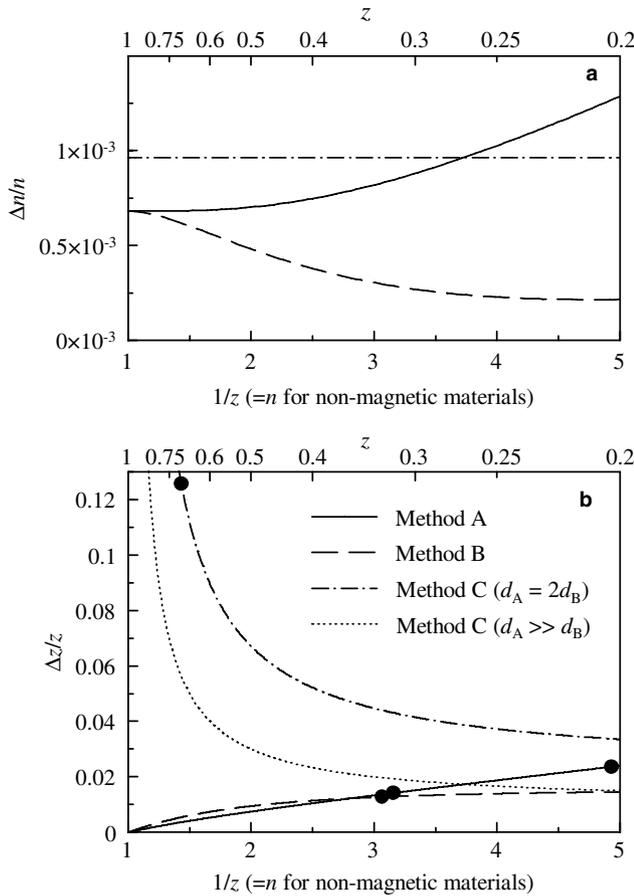
Fig. 5. Relative errors $\Delta n/n$ (a) and $\Delta z/z$ (b) versus reciprocal impedance for the three methods discussed in the text assuming real n and z. (a) Plots based on Eqs. (9)–(11); $f = 1$ THz; $nd = 0.7$ mm and $n(d_A - d_B) = 0.7$ mm. (b) Plots based on Eqs. (14), (15) and (17), valid for any frequency and sample thickness. The errors in the determination of the transmittance ($|\Delta T_m/T_m|$) and reflectance ($|\Delta R_0/R_0|$) spectra are assumed to be independent and equal to 0.01. The sample thickness is assumed to be exactly determined. Points on the curves represent expected errors for the samples studied in this work assuming $|\Delta T_m/T_m| = |\Delta R_0/R_0| = 0.01$.

The permittivity and permeability can be expressed respectively as the ratio and product of refractive index and impedance. Their accuracy is thus controlled by the quantity obtained with the least precision, i.e., by the impedance in our case. Improvement of the impedance accuracy is thus of prime importance. For this reason, we compare the presented experimental approaches from the point of view of the sensitivity of z to the errors in the measured T_m and R_0 spectra. In the THz range, for a large majority of materials, $\varepsilon > \mu$, i.e., the impedance is comprised between 0 and 1. For clarity we restrict our discussion to this interval, even if, based on the formulae given below, it can be easily extended to any value of z. When we speak about low-impedance compounds we refer to materials with $z \approx 0.2$; by high-impedance compounds, materials with $z \approx 0.75$ are meant.

Concerning method A for small incidence angles, Eq. (3) can be applied. Differentiation of (3) leads to the following estimation of the errors:

$$\frac{\Delta z}{z} \approx \frac{\Delta R_0}{R_0} \frac{z^2 - 1}{2z}. \tag{14}$$

The variation of the relative error $\Delta z/z$ versus $1/z$ is shown by the solid line in Fig. 5 assuming a real z and a 1% error in the reflectance determination ($|\Delta R_0/R_0| = 0.01$). For the investigated ZnTe sample, the last multiplicative term appearing in the right-hand side of Eq. (14) amounts approximately to 1.5 while $|R_0| \approx 0.5$. Consequently, Eq. (14) accounts for the noise level of $\Delta z \approx 0.01$–0.02 observed in Fig. 1. Note also in Fig. 5 that $\Delta z/z$ is smaller for higher values of impedance, so it is about two times higher for TmFeO$_3$ than for ZnTe.

The situation is slightly more complex for method B. First, let us assume that the thickness of the sample is exactly known. One then finds using Eq. (6):

$$\frac{\Delta z}{z} \approx \left[3\frac{\Delta T_0}{T_0} - \frac{\Delta T_1}{T_1} \right] \frac{1 - z^2}{2(1 + z^2)}. \tag{15}$$

The variation of the relative error $\Delta z/z$ versus $1/z$ is shown by the dashed line in Fig. 5 assuming that errors in the determination of T_0 and T_1 are independent and equal to 0.01. Numerically, this leads to similar values of Δz as in the previous case, at least for low frequencies. In reality, namely for absorbing samples, the relative error in T_1 is expected to be larger than that in T_0.

Now, let us study the effect of the uncertainty in the sample thickness Δd. One finds:

$$\frac{\Delta z}{z} \approx 2\pi i f \Delta d/c \frac{1 - z^2}{1 + z^2}. \tag{16}$$

This may introduce a systematic error which increases with frequency and reaches about 0.01 at 2 THz for an error as small as 1 µm in the absolute sample thickness determination.

Finally, we investigate the last method (C) which is also critically dependent on the determination of the sample thicknesses. First, we assume that the thicknesses of both samples are exactly known. Differentiation of Eq. (8) then leads to:

$$\frac{\Delta z}{z} \approx \left[\alpha \frac{\Delta T_{B,0}}{T_{B,0}} + \beta \frac{\Delta T_{A,0}}{T_{A,0}} \right] \frac{1 + z}{1 - z}, \tag{17}$$

where $\alpha = d_A/(d_A - d_B)$ and $\beta = d_B/(d_B - d_A)$. It clearly appears that the thicknesses of the two samples have to be chosen quite different from each other to minimize the error. In this study we have chosen $d_A \approx 2d_B$, i.e., $\alpha \approx 2$ and $\beta \approx -1$.

The term $(1 + z)/(1 - z)$ in Eq. (17) can take values from about 1.5 for materials with a low z to nearly 10 for high-impedance samples (cf. dotted line in Fig. 5). We clearly see in Fig. 5 that high-impedance samples (like teflon chosen for our study) exhibit a considerably higher experimental error Δz than low-impedance ones. Indeed, for low-impedance samples the magnitude of the experimental error in Δz is found to be nearly comparable to that obtained in the analysis of method B, while for high-impedance samples
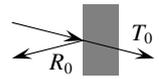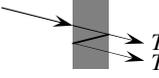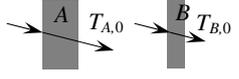
Scheme	Experiment	Precision	Sample thickness
T_0 R_0	Two different setups required	Good	To be optimized for T_0
T_0 T_1	Very simple; parasitic echoes should be avoided	Good at low frequencies; (can be worse at high frequencies)	– To be optimized for T_0 and to avoid excessive attenuation of T_1 – Precise knowledge is essential
A $T_{A,0}$ B $T_{B,0}$	Two samples required	Medium; bad at high frequencies and/or for low impedance	Precise knowledge is essential

Fig. 6. Summary of specific properties of the three approaches presented in this article. (In the schemes, the THz beam is represented with oblique incidence only for graphical clarity; all transmittance measurements are performed under normal incidence.)

it may increase by a factor of 10. This is observed in Fig. 4 where the magnitude of Δz reaches 0.1 even for low frequencies.

The uncertainty in the thickness of sample A (Δd_A) can be accounted for using the development

$$\Delta z = \frac{\partial z}{\partial d_A} \Delta d_A$$

of Eq. (8). This yields:

$$\frac{\Delta z}{z} \approx \Delta d_A \frac{d_B}{d_A - d_B} \frac{2\pi i n f}{c} \frac{1+z}{1-z}. \tag{18}$$

Again, the systematic error introduced by this term will be significant especially for high-impedance compounds and it increases for high frequencies. We come to the same conclusion as above that the two samples should have quite different thicknesses to minimize the experimental error.

The main features of the three experimental methods discussed above are summarized in Fig. 6.

In our experiments the smallest variation of the magnetic permeability detectable in the impedance spectrum is about 0.1. We have seen that this is not sufficient to determine unambiguously the dielectric versus magnetic character of the resonance observed in $TmFeO_3$ which is too weak ($\Delta\mu \approx 0.02$). On the other hand, we would like to point out that all the methods developed in this paper are directly applicable to investigation of metamaterials, including left-handed media, as long as the typical size of the unit cell is much smaller than the wavelength [17,19]. In this case it is not necessary to consider the multiple reflections from each motif, since the metamaterial can be described using an effective permittivity and permeability. The characterization of the electromagnetic properties of such a structure then requires an independent determination of both these quantities. The sensitivity of the methods developed in this paper seems to be sufficient for metamaterials which exhibit the negative refraction and which necessarily present a spectral range with negative effective permeability.

5. Conclusion

We have proposed and demonstrated three methods which can be used for simultaneous determination of the dielectric and magnetic functions from the transmittance and reflectance spectra. All these methods take advantage of the phase sensitivity and of the possibility of temporal windowing of TDTS. Their common property – the possibility of an accurate determination of the complex refractive index and a less accurate determination of the complex wave impedance – was discussed. The differences among these methods are summarized in Fig. 6. It should be also pointed out that all these methods can be applied to the characterization of both classical materials and metamaterials exhibiting complex behavior of dielectric and magnetic functions, as long as the features in the spectra of the complex wave impedance exceed the noise level.

Acknowledgements

References

[1] D.H. Auston, K.P. Cheung, P.R. Smith, Appl. Phys. Lett. 45 (1984) 284.
[2] G. Grüner (Ed.), Millimeter and Submillimeter Wave Spectroscopy of Solids, Springer-Verlag, Berlin Heidelberg, 1998.
[3] C.A. Schmuttenmaer, Chem. Rev. 104 (2004) 1759.
[4] D. Mittleman, Sensing with Terahertz Radiation, Springer-Verlag, Berlin, 2003.
[5] G. Srinivasan, A.N. Slavin (Eds.), High Frequency Processes in Magnetic Materials, World Scientific, Singapore, 1995, p. 56.
[6] A.A. Mukhin, A.Y. Pronin, A.S. Prokhorov, G.V. Kozlov, V. Železný, J. Petzelt, Phys. Lett. A 153 (1991) 499.
[7] R.W. Sanders, R.M. Belanger, M. Motokawa, V. Jaccarino, S.M. Rezende, Phys. Rev. B 23 (1981) 1190.
[8] K.M. Häussler, J. Brandmüller, L. Merten, H. Finsterhölzl, A. Lehmeyer, Phys. Stat. Sol. B 117 (1983) 225.
[9] A.A. Mukhin, B. Gorshunov, M. Dressel, C. Sangregorio, D. Gatteschi, Phys. Rev. B 63 (2001) 214411.
[10] K.N. Kocharyan, M.N. Afsar, I.I. Tkachov, IEEE Trans. Magn. 35 (1999) 2104.
[11] K.N. Kocharyan, M.N. Afsar, I.I. Tkachov, IEEE Trans. Microwave Theory Techol. 47 (1999) 2636.
[12] S.W. McKnight, L. Carin, C. Vittoria, S.F. Wahid, K. Agi, D. Kralj, IEEE Trans. Magn. 32 (1996) 372.
[13] V.G. Veselago, Sov. Phys. Usp. 10 (1968) 509.

[14] J.B. Pendry, A.J. Holden, D.J. Robbins, W.J. Stewart, IEEE Trans. Microwave Theory Technol. 47 (1999) 2075.

[15] J.B. Pendry, Phys. Rev. Lett. 85 (2000) 3966.

[16] R.A. Shelby, D.R. Smith, S. Schultz, Science 292 (2001) 77.

[17] D.R. Smith, J.B. Pendry, M.C.K. Wiltshire, Science 305 (2004) 788.

[18] D.R. Fredkin, A. Ron, Appl. Phys. Lett. 81 (2002) 1753.

[19] T.J. Yen, W.J. Padilla, N. Fang, D.C. Vier, D.R. Smith, J.B. Pendry, D.N. Basov, X. Zhang, Science 303 (2004) 1494.

[20] H.O. Moser, B.D.F. Casse, O. Wilhelmi, B.T. Saw, Phys. Rev. Lett. 94 (2005) 063901.

[21] K. Aydin, K. Guven, M. Kafesaki, L. Zhang, C.M. Soukoulis, E. Özbay, Opt. Lett. 29 (2004) 2623.

[22] D.R. Smith, S. Schultz, P. Markoš, C.M. Soukoulis, Phys. Rev. B 65 (2002) 195104.

[23] L. Duvillaret, F. Garet, J.-L. Coutaz, Appl. Opt. 38 (1999) 409.

[24] D. Grischkowsky, S. Keiding, M.V. Exter, C. Fattinger, J. Opt. Soc. Am. B 7 (1990) 2006.

[25] L. Duvillaret, F. Garet, J.-L. Coutaz, IEEE J. Sel. Top. Quant. 2 (1996) 739.

[26] T.-I. Jeon, D. Grischkowsky, Appl. Phys. Lett. 72 (1998) 2259.

[27] A. Pashkin, M. Kempa, H. Němec, F. Kadlec, P. Kužel, Rev. Sci. Instrum. 74 (2003) 4711.

[28] P. Kužel, J. Petzelt, Ferroelectrics 239 (2000) 949.

[29] A. Nahata, A.S. Weling, T.F. Heinz, Appl. Phys. Lett. 69 (1996) 2321.

[30] R.E. Denton, R.D. Campbell, S.G. Tomlin, J. Phys. D: Appl. Phys. 5 (1972) 852.

[31] H. Němec, P. Kužel, F. Garet, L. Duvillaret, Appl. Opt. 43 (2004) 1965.

[32] Y. Ino, R. Shimano, Y. Svirko, M. Kuwata-Gonokami, Phys. Rev. B 70 (2004) 155101.

[33] M. Khazan, R. Meissner, I. Wilke, Rev. Sci. Instrum. 72 (2001) 3427.

[34] A. Pashkin, E. Buixaderas, P. Kužel, M.-H. Liang, C.-T. Hu, I.-N. Lin, Ferroelectrics 254 (2001) 113.

[35] L. Duvillaret, F. Garet, J.-L. Coutaz, J. Opt. Soc. Am. B 17 (2000) 452.

[36] G. Gallot, J. Zhang, R.W. Mcgowan, T.-I. Jeon, D. Grischkowsky, Appl. Phys. Lett. 74 (1999) 3450.